J Mater Sci: Mater Electron (2018) 29:628–636
DOI 10.1007/s10854-017-7955-6

CrossMark

Dopant induced band gap broadening and conductivity enhancement of Al doped $Zn_{0.85}Ca_{0.15}O$ thin films

Nripasree Narayanan[1] · N. K. Deepak[1]

Received: 26 July 2017 / Accepted: 3 October 2017 / Published online: 11 October 2017
© Springer Science+Business Media, LLC 2017

Abstract Influence of Al doping on the properties of band gap engineered Ca^{2+} substituted ZnO thin films were investigated. Al doped $Zn_{0.85}Ca_{0.15}O$ films were prepared on glass substrates by spray pyrolysis technique and obtained lower resistivity (~ 10^{-3} Ωcm) and widened band gap. Films were polycrystalline and showed hexagonal wurtzite structure irrespective of doping. Due to the textured growth, crystallinity first improved and then decreased. Elemental analysis confirmed the incorporation of Ca and Al in ZnO lattice. Optical transmission in the visible and near infrared region varied in accordance with crystallinity and degradation at higher doping level is related to the scattering of photons by various disorders and to free carrier absorption. Optical energy gap increased with doping concentration due to Burstein-Moss effect as evident from Hall measurements. At higher doping level, carrier concentration and mobility decreased due to the limit of solid solubility and ionized impurity scattering respectively, but energy gap increased due to high polycrstallinity.

1 Introduction

Transparent and conducting oxide (TCO) thin films are now attracting the interest of materials scientists and developers of new thin film based optoelectronic devices because of their unparalleled characteristics such as tunable electrical conductivity and tailorable optical energy gap. Nowadays, TCO thin films are an integral part of functional devices such as thin film solar cells, light emitting diodes (LEDs), photodetectors, flat panel displays, optical waveguides, window defrosters, thin film transistors, surface acoustic wave (SAW) devices, gas sensors etc. [1–9]. Even though search for good quality TCOs succeeded in part, lack of highly conducting p type materials is still a serious difficulty for the further development in these fields. Most widely used TCOs are indium oxide (In_2O_3), tin oxide (SnO_2), zinc oxide (ZnO), etc. which are n type semiconducting materials intrinsically due to the presence of some stoichiometric defects.

In the present scenario ZnO is the most prominent candidate in the field of optoelectronics because it is abundant and less expensive compared to other TCOs. ZnO attracted substantial interest due to its large optical energy gap (~ 3.37 eV at room temperature) which makes it suitable for blue and ultraviolet applications. The presence of large exciton binding energy (~ 60 meV) leads to lasing action based on exciton recombination even at room temperature. The n type semiconducting behaviour of ZnO is attributed to the presence of intrinsic defects such as zinc interstitials or oxygen vacancies. By controlling the extrinsic doping concentration, the electrical characteristics can be varied from insulating to metallic via semiconducting. Doping with group III elements (B, Al, Ga, etc.) enhances the n type electrical conductivity while group I (Li, Na, etc.) or group V (N, P, As etc.) elements results in p type electrical conductivity. Likewise, the optical energy gap can be engineered to obtain intermediate band gaps by making alloys with other oxide materials having different band gap to be suitable for different optoelectronic applications [10]. For example alloying with MgO ($E_g = 7$ eV) increases the band gap while CdO ($E_g = 2.18$ eV) leads to a decreased energy gap value [11, 12].

Thin films of ZnO can be deposited by a large number of deposition techniques such as sputtering, spray pyrolysis,

✉ N. K. Deepak
dr.deepaknk@yahoo.com

[1] Department of Physics, Kannur University, Kannur, Kerala 670327, India

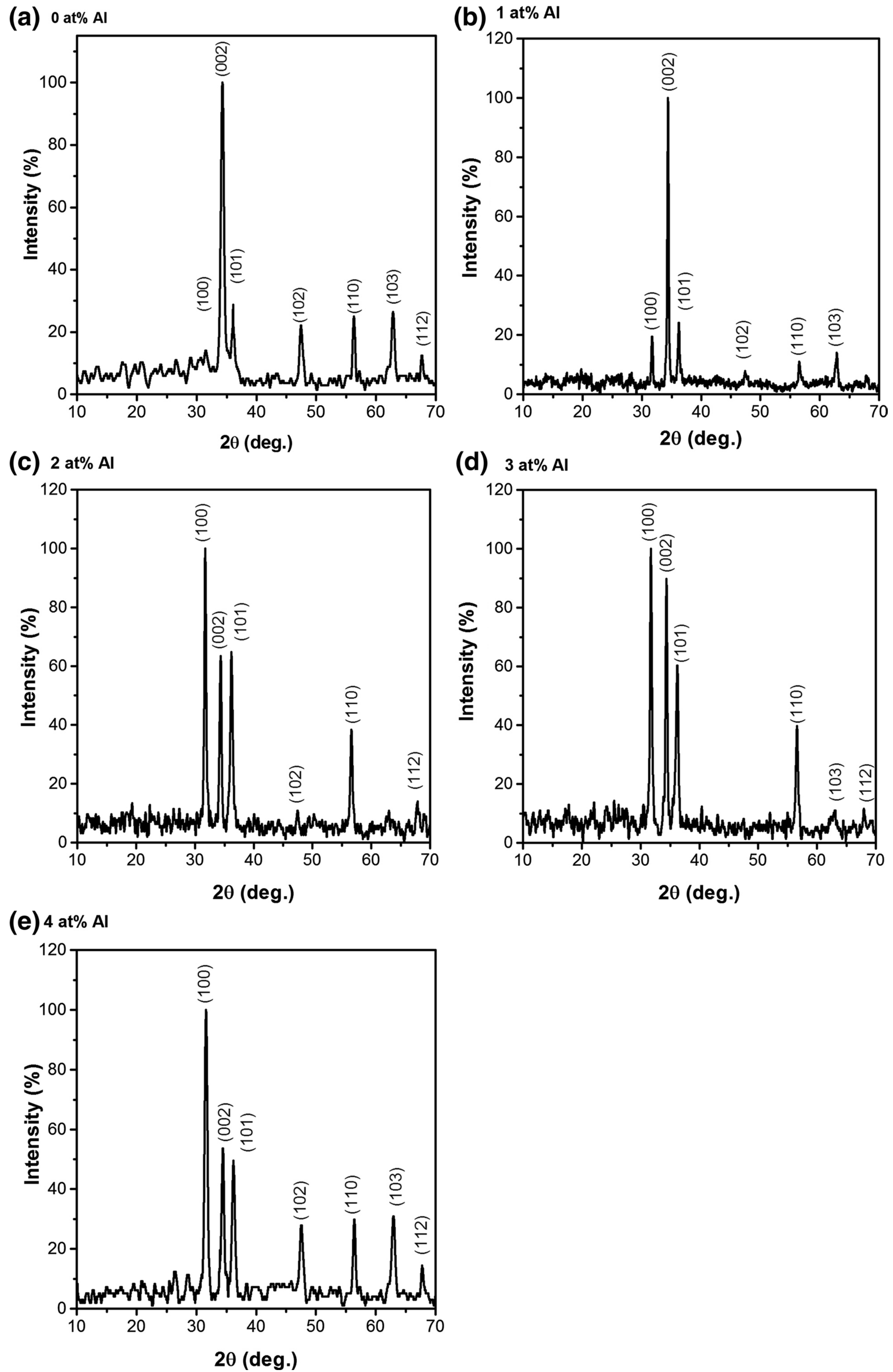

Fig. 1 XRD patterns of Al doped $Zn_{0.85}Ca_{0.15}O$ thin films with 0–4 at% Al doping

chemical vapour deposition (CVD), chemical bath deposition (CBD), atomic layer deposition (ALD), pulsed laser deposition (PLD), spin coating, dip coating etc. Among these spray pyrolysis is a simple and low cost method in which there is no need of vacuum at any stage of deposition and doping can be easily done by adding the salts of the desired dopants into the precursor solution at the time of preparation. In the present study, the influence of aluminium doping on the performance of calcium substituted ZnO thin films were investigated.

2 Experimental methods

0–4 at% Al doped $Zn_{0.85}Ca_{0.15}O$ thin films were deposited on glass substrates by spray pyrolysis (Holmarc HO-TH-04) technique at a substrate temperature of 400 ± 10 °C. Details of the deposition system and conditions were reported elsewhere [13]. The particular stoichiometric composition of $Zn_{0.85}Ca_{0.15}O$ was preferred for the present study because thin film of this composition resulted in promising physical properties in our previous study without showing any secondary phase corresponding to CaO [13]. With 20% Ca^{2+} substitution we obtained new reflection peaks of CaO and concluded that the solubility of Ca^{2+} in ZnO host lattice was below 20%. Misra et al. [14] also reported the synthesis of monophasic $Zn_{(1-x)}Ca_xO$ thin films with x = 0–0.15 by sol–gel spin coating technique. 0.4 M solution composed of zinc acetate dihydrate [$Zn(CH_3COO)_2$. $2H_2O$] and calcium acetate monohydrate [$Ca(CH_3COO)_2$. H_2O] was used as the stock solution for $Zn_{0.85}Ca_{0.15}O$. 1–4 at % Al doping was achieved by adding equivalent quantity of aluminium chloride hexahydrate ($AlCl_3$. $6H_2O$) in the as prepared precursor of $Zn_{0.85}Ca_{0.15}O$. Structural analysis of the films by X-ray diffraction was carried out with Rigaku Miniflex 600 X-ray Diffractometer operating at a voltage of 40 kV using Cu-K_α (λ = 1.5406 Å) radiation. The morphological and composition analyses were performed with JEOL Model JSM – 6390 scanning electron microscope attached with JEOL Model JED – 2300 operated at 20 keV. The optical transmittance spectra of the films were recorded with JASCO V-650 double beam spectrophotometer. The optical gap was derived from the absorbance spectra. Photoluminescence (PL) properties were investigated with Perkin Elmer Fluorescence Spectrometer (LS 55) using an excitation source of wavelength 285 nm. Electrical studies were done using Hall measurement system (Ecopia Hall Effect Measurement System) with a magnetic field strength of 0.55T at room temperature with Van der Pauw configuration. Highly conducting silver paste was used to make ohmic contacts at the four corners in the Van der Pauw geometry. These contacts were then properly heated and allowed to dry to carry out electrical characterization.

3 Results and discussions

3.1 Structural properties

X-ray diffraction (XRD) analysis provides structural mapping of materials. XRD patterns of the Al doped $Zn_{0.85}Ca_{0.15}O$ thin films with varying Al doping percentage were presented in Fig. 1. The samples showed no deviation from the hexagonal wurtzite geometry assumed by ZnO thin films (JCPDS 36-1451). Also the films showed no definite peaks corresponding to the impurity phases. Thus all the films are monophasic and also polycrystalline. The undoped $Zn_{0.85}Ca_{0.15}O$ showed a preferred orientation along the (002) plane with an average crystallite size of 13.16 nm [13]. With 1 at% Al incorporation, (100) peak newly appeared in the XRD pattern, but remained with (002) as the preferred orientation. Since, the ionic radii of Zn^{2+} and Al^{3+} are 74 and 54 pm respectively [15], aluminium can be easily substituted at zinc sites and can improve the preferred growth along [002] direction. When the doping level increased, preferential orientation shifted to (100) plane. This indicates the switching of growth of grains from the c-axis perpendicular to the substrate surface to other directions as the nucleation rates are different along different directions for different doping levels. This can be elucidated in terms of the change in surface energy density above the critical level of Al doping. It was previously reported by some authors that the preferred orientation changes beyond certain doping level called critical doping level or solubility limit [16–21]. Doping beyond the solubility limit results not only in stacking of defects and loss in periodicity in the ZnO lattice but also in segregation of excess Al atoms and formation of non-conductive neutral defects such as Al_2O_3 around the grain boundaries [17, 22]. This will alter the energetic balance between (002) and (100) orientations and induce weakening of (002) peak and building up of crystallites along random directions. Thus it is obvious that the doping percentage controls and modifies the grain growth and hence the evolution of microstructure.

Table 1 Average crystallite size (D), energy gap (E_g) and Burstein-Moss energy shift (E_{BM}) of Al doped $Zn_{0.85}Ca_{0.15}O$ thin films with different Al concentrations

Al concentration (at%)	D (nm)	E_g (eV)	E_{BM} (eV)	Reference
0	13.16	3.505	–	[13]
1	22.69	3.570	0.211	Present study
2	22.14	3.601	0.568	Present study
3	13.33	3.623	0.559	Present study
4	11.41	3.657	0.258	Present study

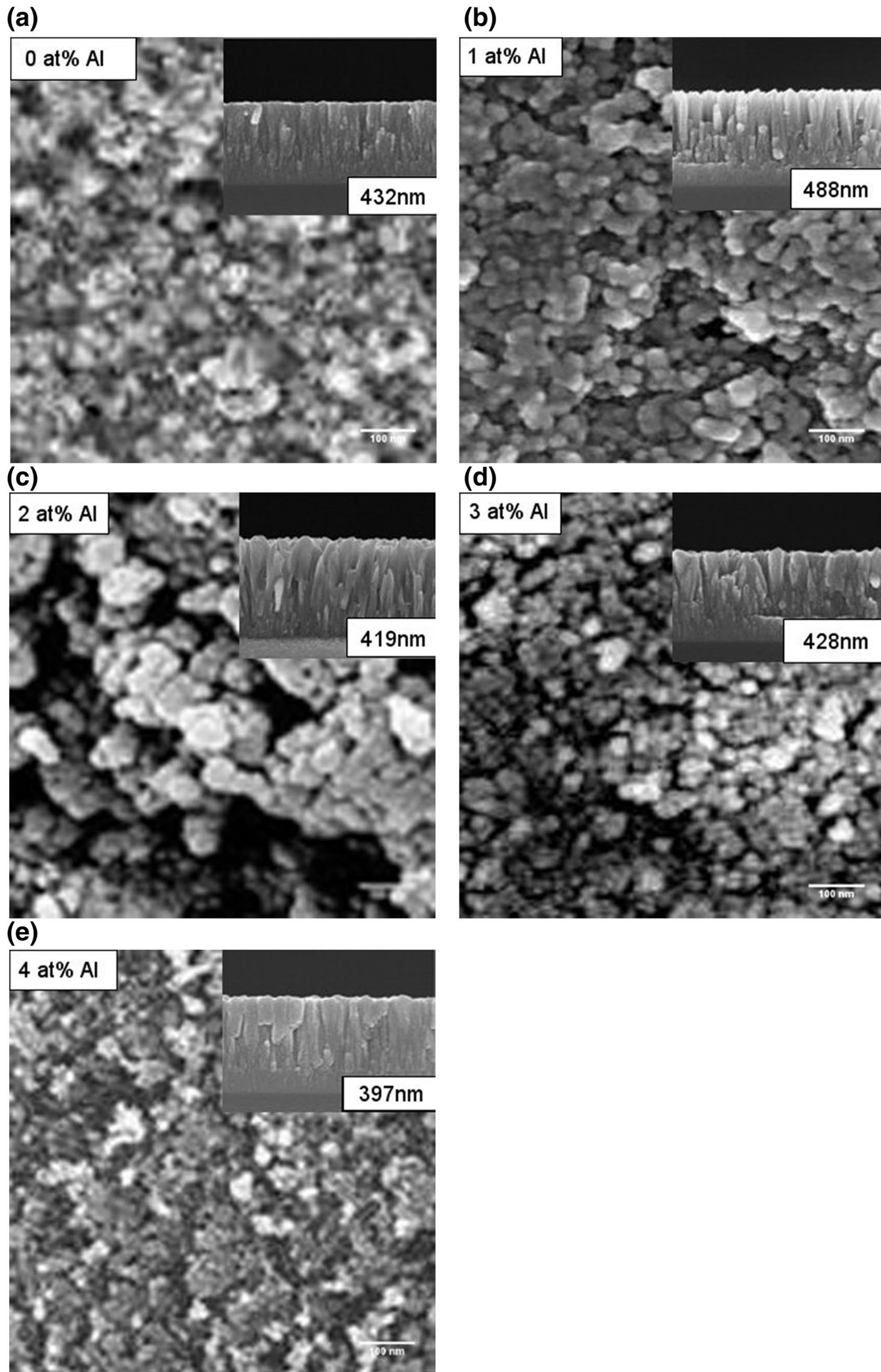
(a)
0 at% Al
432nm
100 nm
(b)
1 at% Al
488nm
100 nm
(c)
2 at% Al
419nm
(d)
3 at% Al
428nm
100 nm
(e)
4 at% Al
397nm
100 nm

◂**Fig. 2** SEM images of Al doped $Zn_{0.85}Ca_{0.15}O$ thin films with 0–4 at% Al doping. In the inset cross-sectional SEM images of each sample was presented

An estimation of the average (mean) crystallite size (D) has been done using the well known formula of Scherrer [23]:

$$D = \frac{0.9\lambda}{\beta \cos\theta} \tag{1}$$

where β is the observed angular width at half maximum intensity (FWHM) of each diffraction peak located at a peak position 2θ and λ is the X-ray wavelength (1.5406 Å). Table 1 summarises the values of crystallite size of ZnO thin films fabricated using different concentrations of Al dopant in the starting solution. The crystallinity first improved with Al doping due to the preferred growth of grains. Further increase in Al concentration deteriorated the crystallinity. Stress induced in the crystallites due to the difference in ionic radii between Zn^{2+} and Al^{3+} and the segregation of Al_2O_3 inhibit the growth of grains and densify grain boundaries [24]. Moreover, the pinning force exerted on the grain boundaries by the defects formed by Al doping restrict the growth of grains and hence result in poor crystallinity.

3.2 Morphological and compositional analysis

Scanning electron microscope (SEM) images, shown in Fig. 2 reveals uniform nanocrystalline nature of the films with different Al doping concentrations. Visual appearance of the micrographs makes sure that the grains are several times larger than the mean crystallite sizes estimated by Scherrer formula for the most intense peak in the diffraction data. This could be due to the formation of grains comprising more than one crystallite. Also there is no visible variation in the microstructure with doping level. Cross-sectional SEM images of the 0–4 at% Al doped $Zn_{0.85}Ca_{0.15}O$ thin films were shown in the inset of Fig. 2 and the measured thickness values were shown in the images. It was observed that the film thickness slightly modified with 1 at% Al doping which could be due to the extremely strong textured growth of crystallites along the (002) plane, c axis normal to the substrate surface, compared to the undoped sample. Increase in Al doping decreased the film thickness and no general trend was followed in the thickness values at higher doping levels. This decrease might be due to the shift in preferential orientation from [002] to [100] direction as seen from the XRD as well as the incorporation of Al^{3+} ions with lower ionic radius at Zn^{2+} lattice sites with increased addition of dopants. Figure 3 shows the energy dispersive X-ray (EDX) spectra of the samples which confirmed the presence of the dopants in the samples.

3.3 Optical properties

Figure 4 shows the variation of optical transmittance with wavelength in the visible and near infrared (NIR) region of differently Al doped $Zn_{0.85}Ca_{0.15}O$ thin films. The measurements were made in the 300–900 nm spectral region at room temperature. All the films possessed better optical transmission, initially increased and thereafter decreased with increase in Al doping percentage (Fig. 5). The observed increase is related to the improvement in cytstallinity while the degradation in transmission could be due to the increased absorption of free carriers. Also the increased scattering of photons created by impurity doping could also be responsible for the observed reduction in transmittance. All the films possessed sharp absorption in the near ultraviolet region corresponding to the inter-band electronic transitions which had undergone a slight blue-shift indicating band gap broadening. According to some early reports, inter-band electronic transitions in ZnO usually involve direct transitions between the bottom of the conduction band constituted predominantly by O 2p states and the top of the valence band formed mainly from Zn 4s states [25, 26]. The absorption coefficient (α) varies with the incident photon energy (hν) and obeys the Tauc relation [27]:

$$\alpha = \frac{B}{h\nu}\left(h\nu - E_g\right)^n \tag{2}$$

where n and B are constants independent of the photon energy and n is equal to ½ as ZnO is a direct band gap material. The estimated band gap energy values were presented in Table 1. The optical energy gap for the undoped sample was estimated to be 3.505 eV [13]. It was observed that the optical energy gap increased with aluminium doping concentration which could be due to the Burstein-Moss effect arising with increase in carrier concentration as evident from the Hall effect measurement. According to Burstein, the magnitude of Burstein-Moss shift (E_{BM}) in energy gap defined as the shift of Fermi level with respect to the bottom of the conduction band can be approximated using the relation [28]

$$E_{BM} \approx \frac{h^2}{8m^*}\left(\frac{3}{\pi}\right)^{2/3} n^{2/3} \tag{3}$$

where h is the Planck's constant, m* is the electron effective mass, and n is the electron density determined from Hall effect measurements. We use $m^* = 0.26\ m_0$ assuming that the bottom of the conduction band is located at the centre of Brillouin zone and therefore the electron effective mass remains unchanged within the occupied part of the conduction band [29, 30]. Band gap energy showed monotonous increase even after the carrier concentration showed saturation at higher doping level. This increase in energy gap can

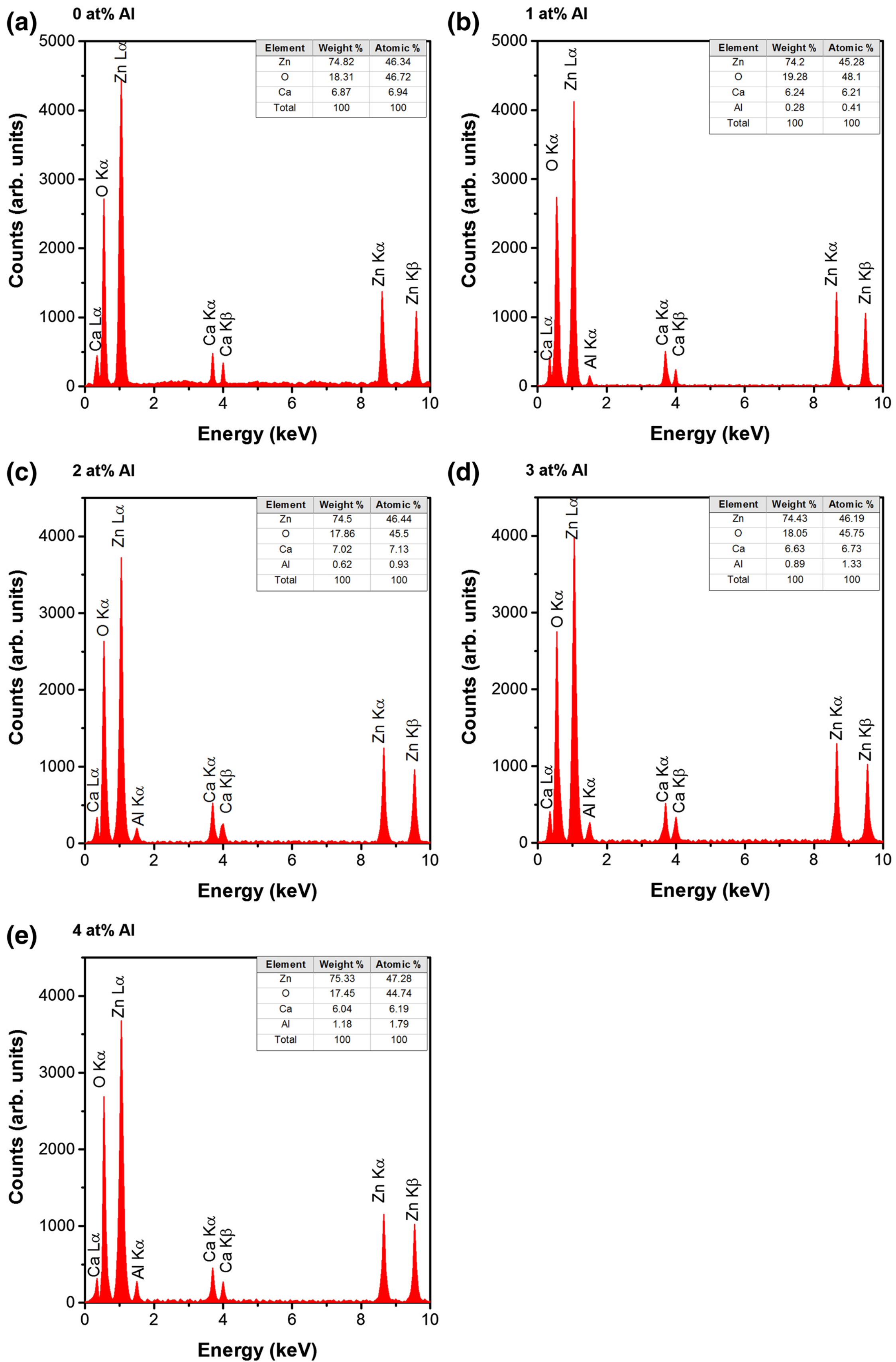

Fig. 3 EDX spectra of Al doped $Zn_{0.85}Ca_{0.15}O$ thin films with 0–4 at% Al doping

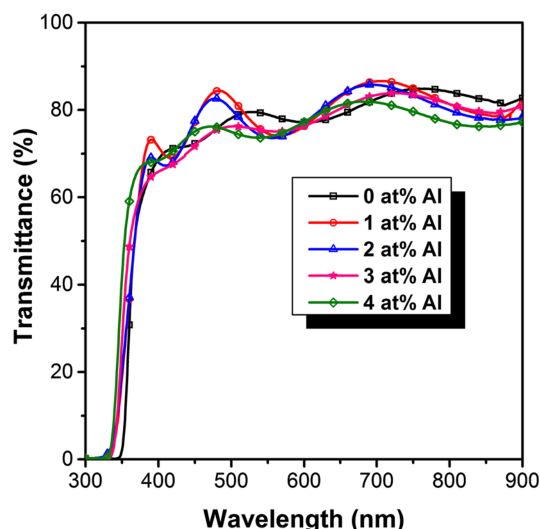

Fig. 4 Transmittance spectra of Al doped $Zn_{0.85}Ca_{0.15}O$ thin films

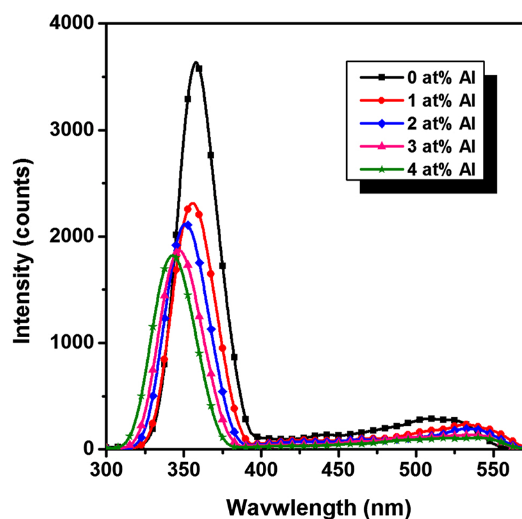

Fig. 6 Room temperature PL spectra of 0–4 at% Al doped $Zn_{0.85}Ca_{0.15}O$ thin films

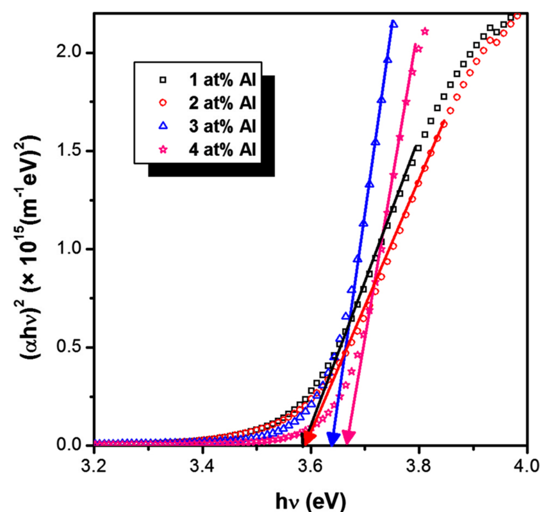

Fig. 5 Tauc plot of 0–4 at% Al doped $Zn_{0.85}Ca_{0.15}O$ thin films for band gap energy (E_g) determination

Table 2 Carrier type, concentration (n), mobility (μ) and resistivity (ρ) of Al doped $Zn_{0.85}Ca_{0.15}O$ thin films with different Al concentrations

Al concentration (at%)	Type	n (cm^{-3})	μ (cm^2/Vs)	ρ (Ωcm)
0	n	7.34×10^{16}	6.38	1.33×10^{1}
1	n	5.84×10^{19}	6.21	1.95×10^{-2}
2	n	2.58×10^{20}	3.54	7.24×10^{-3}
3	n	1.26×10^{20}	8.62×10^{-1}	5.96×10^{-2}
4	n	7.92×10^{19}	1.01×10^{-1}	8.01×10^{-1}

be explained as a consequence of larger extended localization in the valence and conduction bands as a result of segregation of Al_2O_3 around the grain boundaries. In addition, according to Sernelius et al. [31] displacement polarization effects and structural disorders might affect the band tails and cause band gap energy variations.

3.4 Photoluminescence

Figure 6 shows the room temperature PL spectra of 0–4 at% Al doped $Zn_{0.85}Ca_{0.15}O$ thin films which exhibit strong influence of dopants and doping concentration on the emission intensity. Spectra of all the films consist of two emission peaks, one located in the near ultraviolet (UV) region namely near band edge emission (NBE) and the latter in the visible region of the electromagnetic spectrum known as deep level emission (DLE) band. Sharp and intense UV emission band is the intrinsic characteristic of wurtzite ZnO and is arising from the free exciton annihilation from the position of peak energy [32]. High intensity of the NBE peak is strongly correlated with the crystalline quality of the deposited thin films. The visible band in general is originating from transitions between various defect levels present in the forbidden gap and the broadness results from the superposition of emissions from many different defect levels simultaneously. According to the literature, different levels are suggested by different researchers as the origin of various visible emissions. The green emission (~2.17–2.50 eV) can be from intrinsic defects such as zinc interstitials or oxygen vacancies which act as donor defects [33]. Borseth et al. [34] and Zhao et al. [35] reported that more than one defects such as V_O and O_{Zn} may also contribute to this green emission. Kalson et al. [36] on theoretical basis concluded that the

green luminescence is attributed to O_{Zn}. Yellow emission (~2.10–2.17 eV) can be related to the oxygen interstitials which results in an irradiative recombination of an electron from conduction band with hole at this defect level [37, 38]. Meanwhile the orange emission (~1.96–2.10 eV) is accompanied with Zn_i to O_i transitions [39].

It was seen from the spectra that the NBE peaks blue-shifted and intensity gradually decreased with increase in Al doping concentration. The blue-shift of the UV emission band is in accordance with the UV–Vis spectra analysis which showed band gap broadening with increase in doping percentage while the decrease in intensity suggests degradation in crystalline quality as already seen from the XRD analysis. Also the visible emission diminished with Al doping which can be explained as follows. Concentration of zinc interstitials will be reduced for charge compensation in the case of trivalent cation doping [40]. This decreases radiative transitions emitting visible photons and consequently intensity of the band decreases. Moreover, the presence of aluminium dopants in the lattice induce change in rate of growth of crystallites in different directions and changes the diffusion of Zn and O at the surface during deposition and hence a decrease in emission intensity.

3.5 Electrical studies

Electrical properties of the as-deposited thin films were listed in Table 2. Al doping resulted in an enhancement of cattier concentration by four orders of magnitude and consequently a resistivity of the order of ~10^{-3} Ωcm. It was observed that, carrier concentration increased with Al doping except at higher concentrations where the density slightly decreased. The initial increase in electron density is attributed to the substitution of Al^{3+} at Zn^{2+} sites which provides one free electron to the structure. When the doping level is increased, more dopants occupy the cation sites and provide more free electrons. However, after an optimum level of doping, due to the limit of solid solubility, dopants cannot occupy Zn sites and occupy some interstitial sites by forming aluminium oxide [41] and hence ineffective in donating electrons. These excess aluminium segregate at the grain boundaries and create carrier traps in the lattice thereby reducing the carrier concentration and mobility [42].

The carrier mobility decreased with an increase in doping. When a metal dopant substitutes for host metal, the conduction band undergoes perturbation due to the disorders raised by the difference in ionic radii. This increases the possibility of the scattering of conduction electrons by way of mechanisms such as ionized impurity scattering, grain boundary scattering etc. leading to a reduction in the electron mobility. A high carrier concentration of the order of 10^{20} cm^{-3} indicates that the films are degenerate semiconductors which will play a significant role to rule out the chance of grain boundary scattering. Hence we can make a conclusion that the reduction in mobility is mainly related with ionized impurity scattering.

4 Conclusions

Al doped $Zn_{0.85}Ca_{0.15}O$ thin films were prepared on glass substrates by spray pyrolysis method and obtained lower resistive (~10^{-3} Ωcm) transparent and conducting n type thin films. XRD analysis revealed that there was no profound deviation from the hexagonal wurtzite structure in any of the deposited samples and hence the dopants were successfully incorporated in the ZnO lattice. Growth rate of crystallites along different orientations was highly sensitive to dopants and the level of doping. EDX analysis confirmed the presence of calcium and aluminium in the samples in addition to zinc and oxygen. Initially optical transmittance improved with Al doping but at higher concentrations decreased due to increased scattering of photons by various defects and disorders as well as due to the absorption of free carriers. Electron concentration increased up to 2 at% doping and thereafter decreased due to the inefficacy of excess dopants to donate free electrons. Carrier mobility also decreased at higher Al doping mainly due to ionized impurity scattering. Optical energy gap increased monotonously with doping percentage due to Burstein-Moss effect. However, the observed broadening of band gap at 4 at% Al doping with lower electron density was related to the poor crystallinity of the sample.

Acknowledgements First author would like to gratefully acknowledge the University Grants Commission (UGC), New Delhi for providing senior research fellowship (SRF).

References

1. K.L. Chopra, S.R. Das, *Thin Film Solar Cells*. (Plenum Press, New York, 1983)
2. J. Gao, A.J. Heeger, J.Y. Lee, C.Y. Kim, Synth. Mater. **82**, 221 (1996)
3. H.L. Hartnagel, A.L. Dawar, A.K. Jain, C. Jagadish, (Semiconducting Transparent Thin Films (Institute of Physics Publishing, Bristol, 1995)
4. D.S. Ginley, C. Bright, MRS Bull. **25**, 15 (2000)
5. C.G. Granqvist, Sol. Energy Mater. Sol. Cells **91**, 1529 (2007)
6. E. Fortunato, D. Ginley, H. Hosono, D.C. Paine, MRS Bull. **32**, 242 (2007)
7. B.J. Norris, J. Anderson, J.F. Wager, D.A. Keszler, J. Phys. D **36**, L105 (2003)
8. I. Hamberg, C.G. Granquist, J. App. Phys. **60**, R123 (1986)
9. M. Batzill, U. Diebold, Prog. Surf. Sci. **79**, 47 (2005)
10. P. Misra, P.K. Sahoo, P. Tripathi, V.N. Kulkarni, R.V. Nansedkar, L.M. Kukreja, Appl. Phys. A **78**, 37 (2004)
11. Z.J. Othman, A. Matoussi, F. Fabbri, F. Rossi, G. Salviati, Appl. Phys. A **116**, 1501 (2014)

12. S. Sadofev, P. Schäfer, Y.-H. Fan, S. Blumstengel, F. Henneberger, Appl. Phys. Lett. **91**, 201923 (2007)
13. N. Narayanan, N.K. Deepak, Solid State Sci. **71**, 42 (2017)
14. K.P. Misra, R.K. Shukla, A. Srivastava, A. Srivastava, Appl. Phys. Lett. **95**, 031901 (2009)
15. V. Raghavan, *Material Science and Engineering: A First Course*. (Prentice - Hall, New Delhi, 2007)
16. J. Xu, H. Wang, L. Yang, M. Jiang, S. Wei, T. Zhang, Mater. Sci. Eng. B **167**, 182 (2010)
17. C.M. Muiva, T.S. .Sathiaraj, K. Maabong, Ceram. Int. **37**, 555 (2011)
18. B.J. Babu, A. Maldonado, S. Velumani, R. Asomoza, Mater. Sci. Eng. B **174**, 31 (2010)
19. L. Castaneda, R. Silva-Gonzalez, J.M. Gracia-Jimenez, M.E. Hernandez-Torres, M. Avendano-Alejo, C. Marquezbeltran, L. de la Olvera, J. Vega-Perez, A. Maldonado, Mater. Sci. Semiconduct. Process. **13**, 80 (2010)
20. S.B. Sathish, I.S. Mulla, Sens. Actuators B **156**, 943 (2011)
21. S. Tewari, A. Bhattacharjee, Pramana-J. Phys. **76**, 153 (2011)
22. L. Dghoughi, F. Ouachtari, M. Addou, B. Elidrissi, H. Erguig, A. Rmili, A. Bouaoud, Physica B **405**, 2277 (2010)
23. B.D. Cullity, S.R. Stock, *Elements of X-Ray Diffraction*. (Prentice-Hall, New York, 2001)
24. S.B. Majumder, M. Jain, P.S. Dobal, R.S. Katiyar, Mater. Sci. Eng. B **103**, 16 (2003)
25. E.C. Etinorgu, S. Goldsmith, J. Phys. D **40**, 5220 (2007)
26. P.D.C. King, T.D. Veal, A. Schleife, J. Zuniga-Perez, B. Martel, P.H. Jefferson, F. Fuchs, V. Munoz-Sanjose, F. Bechstedt, C.F. McConville, Phys. Rev. B **79**, 205205 (2009)
27. J.I. Pankove, *Optical Processes in Semiconductors*. (Prentice-Hall, Englewood Cliffs, 1971)
28. E. Burstein, Phys. Rev. **93**, 632 (1954)
29. B.E. Sernelius, K.F. Berggren, Z.C. Jin, I. Hamberg, C.G. Granqvist, Phys. Rev. B **37**, 10244 (1988)
30. H.H.-C. Lai, V.L. Kuznetsov, R.G. Egdell, P.P. Edwards, Appl. Phys. Lett. **100**, 072106 (2012)
31. B.E. Sernelius, K.F. Berggren, Z. Jin, I. Hamberg, C.G. Granqvist, Phys. Rev. B **37**, 10244 (1998)
32. P. Zu, Z.K. Tang, G.K.L. Wong, M. Kawasaki, A. Ohtomo, H. Koinuma, Y. Segawa, Solid State Commun. **103**, 459 (1997)
33. K. Vanheusden, C.H. Ceager, W.L. Warren, D.R. Tallant, J.A. Voigt, Appl. Phys. Lett. **15**, 403 (1996)
34. T.M. Borseth, B.G. Svensson, A.Y. Kuznetsov, P. Kalson, Q.X. Zhao, M. Willander, Appl. Phys. Lett. **89**, 262112 (2006)
35. Q.X. Zhao, P. Kalson, M. Willander, H.M. Zhong, W. Lu, J.H. Yang, Appl. Phys. Lett. **87**, 211912 (2005)
36. P. Kalson, T.M. Borseth, Q.X. Zhao, B.G. Svensson, A.Y. Kuznetsov, M. Willander, Solid State Commun. **145**, 321 (2008)
37. O.F. Schirmer, D. Swingel, Solid State Commun. **8**, 1559 (1970)
38. X.L. Wu, G.G. Siu, C.L. Fu, H.C. Ong, Appl. Phys. Lett. **78**, 2285 (2001)
39. H.A. Ahn, Y.Y. Kim, D.C. Kim, S.K. Mohanta, H.K. Cho, J. Appl. Phys. **105**, 013502 (2009)
40. S. Fujihara, A. Suzuki, T. Kimura, J. Appl. Phys. **94**, 2411 (2003)
41. D. Cossement, J.M. Streydio, J. Cryst. Growth **72**, 57 (1985)
42. H. Gomez-Pozos, A. Maldonado, M.D. Olver, Mater. Lett **61**, 1460 (2007)